

This work was written as part of one of the author's official duties as an Employee of the United States Government and is therefore a work of the United States Government. In accordance with 17 U.S.C. 105, no copyright protection is available for such works under U.S. Law.

Public Domain Mark 1.0

<https://creativecommons.org/publicdomain/mark/1.0/>

Access to this work was provided by the University of Maryland, Baltimore County (UMBC) ScholarWorks@UMBC digital repository on the Maryland Shared Open Access (MD-SOAR) platform.

**Please provide feedback**

Please support the ScholarWorks@UMBC repository by emailing [scholarworks-group@umbc.edu](mailto:scholarworks-group@umbc.edu) and telling us what having access to this work means to you and why it's important to you. Thank you.

# ULTRA-LOW-FREQUENCY WAVE POWER IN THE MAGNETOTAIL LOBES

## 1. RELATION TO SUBSTORM ONSETS AND THE AURORAL ELECTROJET INDEX

R. A. Smith<sup>1</sup>, M. L. Goldstein<sup>2</sup>, M. R. Sands<sup>3</sup>, R. P. Lepping<sup>2</sup>, C. K. Goertz<sup>1</sup>, B. G. Harrold<sup>1</sup>,  
C. A. Fitch<sup>2</sup>, and L.-H. Shan<sup>1</sup>

**Abstract.** Time series observations of the magnetotail lobe magnetic field have been Fourier analyzed to compute the frequency-weighted energy density  $P_{fz}$  in the range 1-30 mHz.  $P_{fz}$  is generally observed in the range  $10^{-4}$  -  $10^{-2}$   $\gamma^2$  - Hz, with a mean value of  $1.2 \times 10^{-3}$   $\gamma^2$  - Hz during substorm growth phases and  $1.0 \times 10^{-3}$   $\gamma^2$  - Hz in the comparison intervals. No strong correlation of  $P_{fz}$  is found with AE in either set of intervals, but during substorm growth phases  $P_{fz}$  may vary by an order of magnitude over time scales of 30 min, with a tendency for higher power levels to occur later in the growth phase. Increases in  $P_{fz}$  are seen to precede by ~ 10 min localized expansive phase activity observed in individual magnetograms. The observed levels of  $P_{fz}$  during growth phases are in general accord with the requirements of the thermal catastrophe substorm model.

### Introduction

This is the first in a series of reports on a systematic study of ultra-low-frequency (ULF) waves in the magnetotail lobes. The primary motivation for this investigation is to provide an observational test of the recently emerging thermal catastrophe model of substorm evolution (Smith, Goertz, and Grossmann, 1986; Goertz and Smith, 1989). The fundamental assumption of the thermal catastrophe model is the existence of ULF Poynting flux incident from the lobe onto the plasma sheet boundary layer (PSBL). Plasma convecting through the boundary layer is nonadiabatically heated by resonant Alfvén absorption and subsequently convected to the central plasma sheet (CPS). Recent observations present increasing evidence of nonadiabatic heating during substorm evolution, and during the growth phase in particular (Williams et al., 1990; C. Y. Huang et al., unpublished manuscript, 1989).

The resonant heating rate is proportional to the quantity

$$P_{fz} = \int df f |b_{zf}|^2, \quad (1)$$

the frequency-weighted energy density of the wave magnetic z-component at the interface between the lobe and the PSBL;  $|b_{zf}|$  is the Fourier amplitude of  $b_z$  at frequency  $f$ . Thus, an observational test of the importance of resonant absorption in

substorm evolution is provided by measurements of the ULF spectrum in the appropriate frequency range. The level of  $P_{fz}$  for which substorm dynamics are significantly affected is in the range  $10^{-3}$  -  $10^{-2}$   $\gamma^2$  - Hz (see the discussion below).

### Philosophy and Methodology

To interpret a test of the thermal catastrophe model, it is important to avoid confusion with the near-Earth-neutral-line model (Hones, 1979). In this model, MHD wave activity plays no role in the approach to expansion-phase onset, or in triggering the reconnection process. Once onset occurs — by whatever mechanism — MHD activity may occur due to magnetic reconfiguration and the dynamics associated with enhanced energy dissipation in the substorm sector. The distinctive prediction of the thermal catastrophe model, however, is that the requisite wave power is present in the lobe before onset. Thus the paradigm interval for analysis in our study is the growth phase preceding an isolated substorm or the first in a sequence of repeated substorms. During the growth phases of succeeding substorms in a sequence, significant ULF power observed in the lobes could be postulated to be remnant activity from previous substorms. (See, however, the discussion below of Event 8.) The present results include analyses of thirty-eight such paradigm intervals.

In the thermal catastrophe model, the increase in lobe field strength during the growth phase drives the magnetotail toward the critical configuration for catastrophe. In the context of catastrophe theory, both  $P_{fz}$  and the lobe field strength  $B_l$  are control parameters. Visual inspection of AE reveals frequent periods of sustained geomagnetic activity at moderate levels of AE — typically 200-300  $\gamma$  — with no marked structure. We also selected a set of such intervals for analysis, under the hypothesis that they constitute a comparison group in which the combination of control parameters  $P_{fz}$  and  $B_l$  would be insufficient to cause a substorm. The present results include analysis of eighteen such intervals.

Candidate intervals for analysis were selected on the basis of visual inspection of AE. In the case of ISEE, we confined the search to the months of March and April, when the spacecraft had the highest probability of being in the tail. For IMP 6, which had a highly eccentric orbit, the search was conducted for the months of July through December. To be selected on the basis of AE, an interval must have been immediately preceded by at least one hour during which  $AE < 100 \gamma$  or two hours during which  $AE < 200 \gamma$ . This criterion is designed to prevent analyzing residual MHD activity from previous substorms. The intervals thus selected were subsequently checked for satellite coverage in the lobes.

For the paradigm substorm subset, we searched for isolated substorm signatures exhibiting a growth phase, a sudden onset, and a recovery phase, all clearly identifiable in AE. In these cases, the candidate interval was defined to

<sup>1</sup> Department of Physics and Astronomy, The University of Iowa, Iowa City, IA 52245

<sup>2</sup> Laboratory for Extraterrestrial Physics, NASA Goddard Space Flight Center, Greenbelt, MD 20771

<sup>3</sup> Science Applications International Corporation, McLean, VA 22102

include approximately 0.5 - 1 hr of the geomagnetically quiet period preceding the growth phase and the growth phase up to but not including the time of sudden onset, provided the apparent onset (identified as a sharp increase in AE) occurred at  $AE < 500 \gamma$ . Data were not analyzed for  $AE > 500 \gamma$ . For the comparison set, consisting of intervals of quasi-steady geomagnetic activity at moderate AE with no marked structure, candidate intervals were selected to cover the entire duration of activity, including the rise from quiescent levels of AE.

Using the above criteria, of the order of a thousand intervals were tentatively selected for analysis. The minimum allowable length of a data record was taken to be 40 min. Owing to spacecraft trajectories, data gaps, and passages into the PSBL, satellite coverage of the lobe for a usable duration was available for only about 25 percent of the candidate intervals. The criteria used for lobe discrimination were the ion density and magnetic field strength. The lobe field was assumed to have a minimum magnitude of  $20 \gamma$ ; data segments in which the total field strength fell below this magnitude were discarded. Intervals were also discarded if the ion density was greater than  $0.03 \text{ cm}^{-3}$ . The final data set contained 170 intervals (88 from IMP 6 and 82 from ISEE 1), with durations ranging from 40 min to  $\sim 2$  hr. In addition to the paradigm and comparison events described above, the data base contains 120 intervals exhibiting variant morphologies in AE. These will be discussed elsewhere.

For the final set of intervals, the data were inspected visually and purged of interference spikes, which were replaced by linear interpolation using the Interactive Digital Signal Processor package at GSFC. The preprocessed data were subjected to a linear detrend and windowed using a 10% cosine taper, and then Fourier transformed to compute both the conventional power spectra  $|b_j f|^2$  for the individual components ( $j=x,y,z$ ) and the frequency-weighted energy density  $P_f$  for all components, as defined above for  $j=z$ .

## Results

Magnetic field data from representative intervals of both the paradigm (Category 1) and comparison (Category 6) data sets are shown in Fig. 1. Event 8 (numbering is that of the entire data base) is the growth phase of a large substorm for which the onset is indicated by a sharp rise in AE of  $\sim 500 \gamma$  at 0920 UT. This event comprises the longest interval (4 hr) in our data base and is discussed in some detail below. Event 136 is a category 6 event. The AE signatures for these intervals are included in Fig. 3, together with that of a more typical Category 1 event (Event 1). The right panels of Fig. 1 exhibit the power spectra of the individual field components, obtained by spectral analysis of the entire data records for these events, in the range 1-30 mHz.

In preliminary analyses, we calculated the integral (1) for the entire data record of each event. For the substorm events, we noticed an anticorrelation between the values of  $P_{fz}$  thus obtained and the length of the observational record. This led us to consider the hypothesis, not envisioned by our original protocols, that the ULF power of the dominant spectral frequencies may increase over the growth phase. If this were the case, then long observing intervals would bias the calculated powers to lower values than would prevail near and prior to onset. To test this hypothesis, we divided the data records into 20-min tapered windows, sliding the centers of the windows by 10 min, and calculated  $P_{fz}$  in each 20-min interval. The two left panels of Fig. 2 show the relation between  $P_{fz}$  and the corresponding averages of AE for the two event categories. For the substorm events, the powers are also plotted vs. the time before onset ( $t-t_0$ ) at the centers of the windows [Fig. 2(c)]. No correlation between  $P_{fz}$  and either AE or ( $t-t_0$ ) is evident for either category, although there is a weak tendency for the highest powers in the substorm events to occur at high values of AE and closer to onset. This

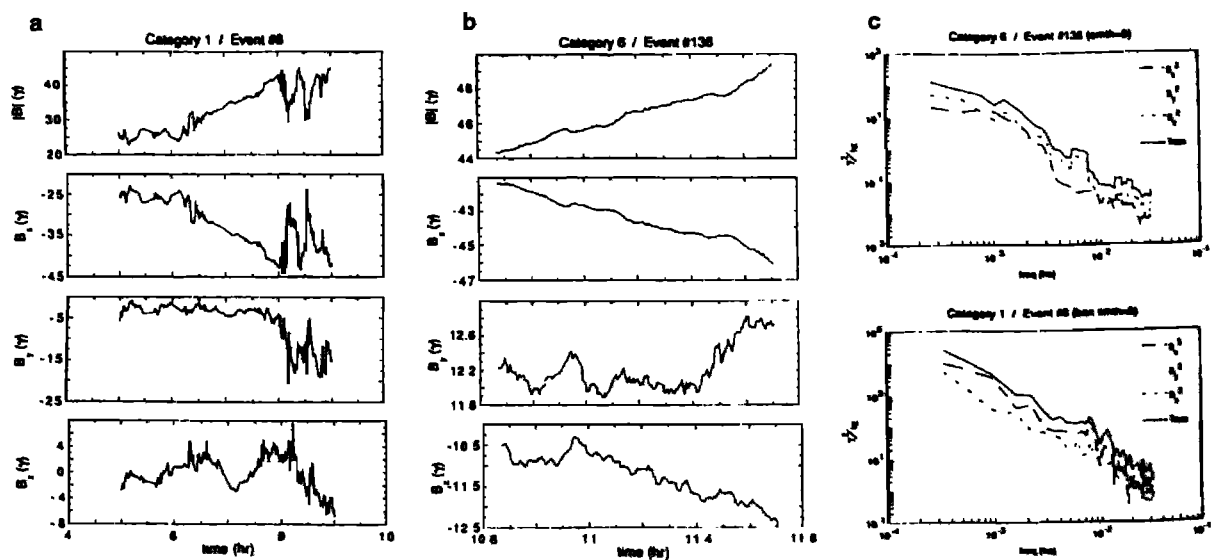


Fig. 1 (a) Magnetic field data during a substorm growth phase (Event 8, Category 1). From top to bottom the panels show the total magnitude and the GSM z, y, and x components, respectively; (b) An interval of prolonged

geomagnetic activity at  $AE \sim 200 \gamma$  (Event 136, Category 6); (c) Power spectra of the detrended field components for the two intervals (top: Event 136).

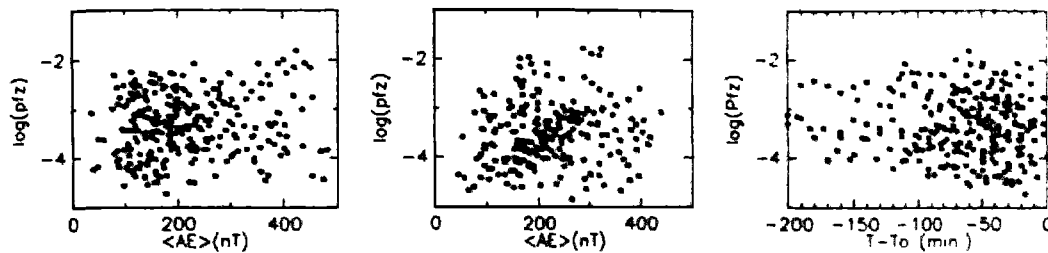


Fig. 2 (a) Occurrence of  $P_{fz}$  vs. the corresponding 20-min averages of AE for substorm growth phases: (b) Same as (a)

for comparison intervals: (c)  $P_{fz}$  vs. time before substorm onset for growth phases.

suggests that ULF wave power in the lobe is not simply related to geomagnetic activity, an indication which is reinforced by consideration of individual events.

In Fig. 3,  $P_{fz}$  is shown vs.  $(t-t_0)$  for the substorm Events 1 and 8 and vs.  $\langle AE \rangle$  for the Category 6 event 136: also shown are the high-resolution AE signatures. For Event 8, the X-component of the ground magnetogram from Fort Churchill is superimposed (with an arbitrary scale) on the plot of  $P_{fz}$  vs.  $(t-t_0)$ . For the “plateau” event 136,  $P_{fz}$  varies by only a factor of 3 over the interval, in a fashion uncorrelated to AE. In contrast, there is a clear correlation between  $P_{fz}$  and  $(t-t_0)$  during the growth phase of Event 1; the correlation with AE appears similar. In Event 8,  $P_{fz}$  has a general increasing trend but varies several times by factors of up to three between successive sliding windows, finally decreasing by an order of magnitude over 40 min in the hour preceding the large onset at 0920.

The relatively unstructured growth phase of Event 8, however, is unusually long. It is rare for a growth phase to proceed for 4 hours with no local expansive phase activity. In Fig. 3, one sees a small but sharp increase in AE at 0530 and a less evident feature at 0740. Overall, however, this AE signature satisfies our selection protocols. It is generally recognized that AE is a conveniently accessible but imperfect indicator of geomagnetic activity. The largest contributions to the driven electrojet tend to occur near dawn and dusk, while expansive-phase activity is generally localized near midnight. Consequently, enhancements of auroral currents that are

localized near midnight and do not produce perturbations above the envelope of the driven system may be masked in AE. In Fig. 3, the Fort Churchill magnetogram reveals two small ( $\sim 200 - 250 \gamma$ ) expansive phase onsets just before 0500 and at 0530, and a larger ( $\sim 300 - 400 \gamma$ ) onset at 0730. None of these events was visible at Great Whale River, one hour to the east (G. Rostoker, private communication, 1990). During this interval, IMP 6 was at  $\sim 0100$  LT. Fort Churchill passed under the spacecraft at  $\sim 0700$  UT. The large onset at 0730 is clearly preceded by an increase in  $P_{fz}$  by a factor of 30 between 0710 and 0730. We have no data before 0500, but the onset at 0530 also appears to be preceded by an increase in  $P_{fz}$  by a factor of 3 between 0510 and 0520. Thus, the increases in wave intensity seen aboard IMP 6 cannot be attributed to the expansive phase onsets.

The spatial distribution of our observations is shown in Fig. 4. Here the plotted symbols indicate the spacecraft position at the start of each observing interval. The gap near GSE  $z = 0$  confirms the discrimination of the lobe, the few points near  $z = 0$  occurring when the plasma sheet is expected to be hinged out of the ecliptic. The distributions are similar for the substorm and comparison intervals. Figure 4 shows that a substantial fraction of the intervals (17%) occurs at  $|z| > 10 R_E$ . Numerical calculations of the propagation of ULF waves generated by sheared magnetosheath flow in a slab model show that the wave power evanescences by about an order of magnitude between the magnetosheath and the PSBL (Harrold et al., 1990). (These calculations also show that at

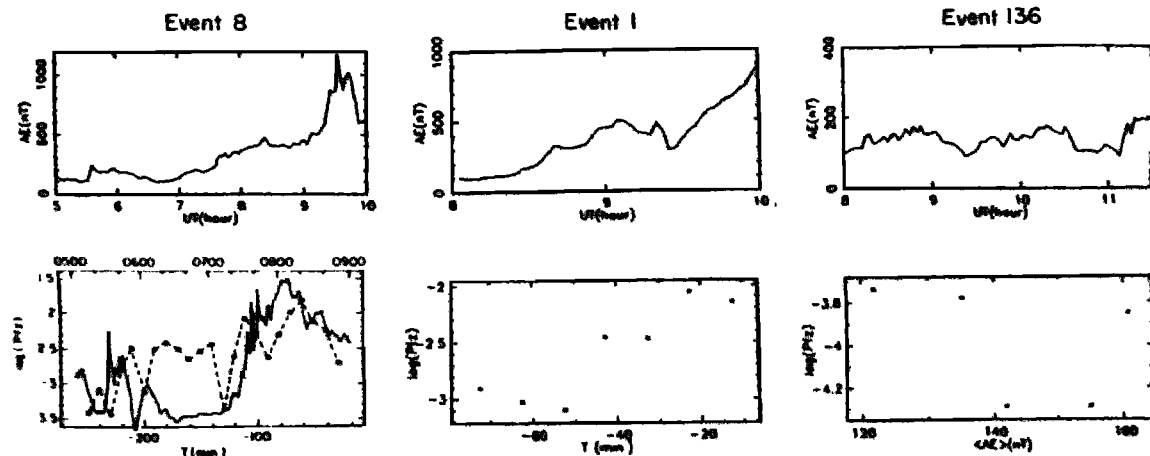


Fig. 3 Top panels: high-time-resolution AE; Bottom panels:  $P_{fz}$  vs. time before onset for Events 8 and 1, and vs.  $\langle AE \rangle$  for

Event 136. For Event 8, the X-component of the ground magnetogram at Fort Churchill is superimposed.

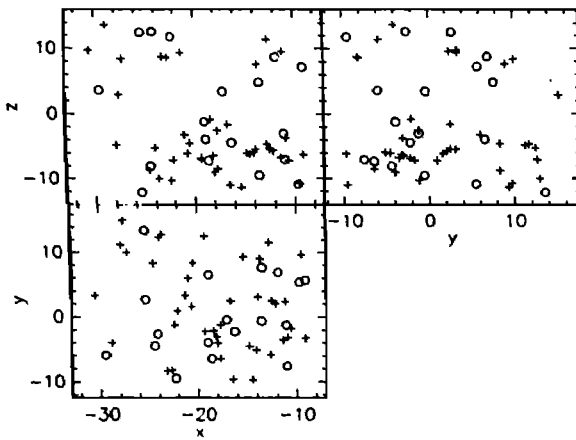


Fig. 4 Spatial distribution of observing positions for Category 1 (crosses) and 6 (circles) events.

all  $|z|$ ,  $P_{fz} > P_{fx}, P_{fy}$ , a result seen in our observational study.) The profile of  $P_{fz}$  in  $z$  is sensitive to the radius of the tail. Thus we cannot make a precise statement about the ratios of our individual observations of  $P_{fz}$  to the corresponding values delivered to the PSBL, but our numerical results indicate that in general the values at the PSBL will be somewhat lower than observed in the lobe. In the future we shall report on the correlation of  $P_{fz}$  with observational position, although from the present results we may expect that this aspect of our study will be complicated by the observed variability of  $P_{fz}$  on short time scales.

#### Discussion

We close with a brief consideration of some quantitative implications of these results for the viability of the thermal catastrophe model. For a given value of  $P_{fz}$ , the Poynting flux incident on the PSBL can be estimated from the single-wave numerical solutions of Harrold et al. (1990). In the linearized MHD wave equation for the inhomogeneous magnetotail, the  $z$ -component of the wave magnetic field is represented by  $b_z(r) = |b_z| \exp[i(k_x x + k_y y + \phi(z) - \omega t)]$ . The Poynting flux is given by

$$S_z = \frac{\omega |b_z|^2}{8\pi k^2} \frac{\partial \phi}{\partial z} \rightarrow \frac{1}{4k^2} \frac{\partial \phi}{\partial z} P_{fz} \quad (2)$$

where  $k^2 = k_x^2 + k_y^2$  and the last form in (2) is the spectral generalization of the single-wave model. In the northern (southern) lobe  $\partial \phi / \partial z < 0$  ( $> 0$ ), i.e., the flux is from the magnetosheath toward the plasma sheet. For typical parameters, Harrold et al. (1990) find  $|\partial \phi / \partial z| \sim 0.2 R_E^{-1}$  and  $\max |\partial \phi / \partial z| \sim 0.4 R_E^{-1}$ . The spectrum is only weakly dependent on  $k$ , which has been taken constant in (2). For  $k = 0.2 R_E^{-1}$  and  $P_{fz} = 6 \times 10^{-3} \gamma^2 \text{ Hz}$ , (2) yields a Poynting flux of order  $1 \mu\text{W m}^{-2}$  incident on the PSBL. This flux is completely absorbed in the PSBL and the heated plasma

convected to the plasma sheet: we may estimate the rate of temperature increase in the CPS by setting

$$S_z = \int_{\text{PSBL}} dz n \frac{\partial T}{\partial t} \approx n_0 V_z \Delta T$$

where  $n_0$  is the density at the resonance layer and  $V_z$  is the  $E \times B$  convection velocity. Taking  $S_z \sim 1 \mu\text{W m}^{-2}$ ,  $n_0 \sim 0.1 \text{ cm}^{-3}$ , and  $V_z \sim 25$  (10)  $\text{km s}^{-1}$ , we find  $\Delta T \sim 2.5$  (6)  $\text{keV}$ , consistent with the observations of Huang et al. (unpublished manuscript, 1989). The present results show that the power densities needed to account for such plasma sheet observations by the thermal catastrophe model are commonly observed in the lobe under conditions leading to substorm onset.

**Acknowledgments.** We thank D. H. Fairfield and C. T. Russell for the satellite data used in this study. The Fort Churchill magnetograms were furnished by the Geological Survey of Canada. We are grateful to G. Rostoker for informative discussions of the magnetometer data, and to L. A. Frank and C. Y. Huang for discussions of LEPDEA plasma data. We have also enjoyed stimulating discussions with D. N. Baker and M. G. Kivelson. This work was supported by NASA Grants NAGW-1653 and NAGW-970 at The University of Iowa and a NASA research grant at the Goddard Space Flight Center.

#### References

- Goertz, C. K., and R. A. Smith, The thermal catastrophe model of substorms, *J. Geophys. Res.*, **94**, 6581-6596, 1989.
- Harrold, B. G., C. K. Goertz, R. A. Smith, and P. J. Hansen, Resonant Alfvén wave heating of the plasma sheet boundary layer, *J. Geophys. Res.*, **95**, 15,039-15,046, 1990.
- Hones, E. W., Jr., Transient phenomena in the magnetotail and their relation to substorms, *Space Sci. Rev.*, **23**, 393, 1979.
- Smith, R. A., C. K. Goertz, and W. Grossmann, Thermal catastrophe in the plasma sheet boundary layer, *Geophys. Res. Lett.*, **13**, 1380-1383, 1986.
- Williams, D. J., D. G. Mitchell, C. Y. Huang, L. A. Frank, and C. T. Russell, Particle acceleration during substorm growth phase and onset, *Geophys. Res. Lett.*, **17**, 587-590, 1990.

<sup>1</sup> Department of Physics and Astronomy, The University of Iowa, Iowa City, IA 52245

<sup>2</sup> Laboratory for Extraterrestrial Physics, NASA Goddard Space Flight Center, Greenbelt, MD 20771

<sup>3</sup> Science Applications International Corporation, McLean, VA 22102

(Received: June 22, 1990;

Revised: August 22, 1990;

Accepted: September 18, 1990)